



Exponentially Amplified Magnetic Field Eliminates Disk Fragmentation around Population III Protostars

Shingo Hirano^{1,2}  and Masahiro N. Machida² ¹ Department of Astronomy, School of Science, University of Tokyo, Tokyo 113-0033, Japan; hirano@astron.s.u-tokyo.ac.jp² Department of Earth and Planetary Sciences, Faculty of Science, Kyushu University, Fukuoka 819-0395, Japan

Received 2022 June 17; revised 2022 August 1; accepted 2022 August 1; published 2022 August 12

Abstract

One critical remaining issue that is unclear in the initial mass function of the first (Population III) stars is the final fate of secondary protostars that formed in the accretion disk—specifically, whether they merge or survive. We focus on the magnetic effects on the formation of the first star under a cosmological magnetic field. We perform a suite of ideal magnetohydrodynamic simulations for 1000 yr after the first protostar formation. Instead of the sink particle technique, we employ a stiff equation of state approach to represent the magnetic field structure connecting protostars. Ten years after the first protostar formation in the cloud initialized with $B_0 = 10^{-20}$ G at $n_0 = 10^4$ cm $^{-3}$, the magnetic field strength around the protostars has amplified from pico- to kilo-Gauss, which is the same strength as the present-day star. The magnetic field rapidly winds up since the gas in the vicinity of the protostar (≤ 10 au) has undergone several tens of orbital rotations in the first decade after protostar formation. As the mass accretion progresses, the vital magnetic field region extends outward, and magnetic braking eliminates the fragmentation of the disk that would happen in an unmagnetized model. On the other hand, assuming a gas cloud with a small angular momentum, this amplification might not work because the rotation would be slower. However, disk fragmentation would not occur in that case. We conclude that the exponential amplification of the cosmological magnetic field strength, about 10^{-18} G, eliminates disk fragmentation around Population III protostars.

Unified Astronomy Thesaurus concepts: [Magnetohydrodynamical simulations \(1966\)](#); [Primordial magnetic fields \(1294\)](#); [Population III stars \(1285\)](#); [Star formation \(1569\)](#); [Stellar accretion disks \(1579\)](#); [Protostars \(1302\)](#)

1. Introduction

One of the significant challenges in modern cosmology is the formation process of the first generation of stars, the so-called Population III (Population III) stars. They influence all subsequent star and galaxy evolution in the early universe through their input of ionizing radiation and heavy chemical elements, depending on the final fates of Population III stars (Yoon et al. 2012). There have been no direct observations yet, but the nature of the first stars has been elucidated by theoretical studies, in particular with numerical simulations of increasing physical realism (for recent reviews, Greif 2015). Furthermore, several indirect constraints exhibit the imprint of the first stars: $< 0.8 M_\odot$ low-mass stars capable of surviving to date (e.g., Magg et al. 2018); $\sim 100 M_\odot$ massive binaries, which can be a promising progenitor of BH–BH (black hole) mergers like the gravitational-wave sources (e.g., Kinugawa et al. 2014); and $\sim 10^5 M_\odot$ supermassive stars, which could have left the massive seed BHs of high- z supermassive black holes (SMBHs; e.g., Inayoshi et al. 2020). There is a need to update theoretical models for the formation and evolution of the first stars to predict their observational signature in light of the upcoming suite of next-generation telescopes.

One of the key unresolved issues in first star formation theory is the efficiency of magnetic effects (e.g., magnetic braking). Previous studies have identified several effects assuming primordial star-forming gas clouds have strong magnetic fields: delaying the gas contraction to the host dark matter (DM) mini halo and the first star formation

(e.g., Koh et al. 2021), preventing disk fragmentation with efficient angular momentum transport due to the magnetic field (Machida & Doi 2013; Sadanari et al. 2021), and reducing the protostellar rotation degree, which can also control the final fate of Population III stars (Hirano & Bromm 2018). However, it is known that the primordial magnetic field of the universe (10^{-18} G; Ichiki et al. 2006) is extremely weak compared to the magnetic field of nearby star-forming regions ($\sim 10^{-6}$ G). Magnetic field amplification by flux freezing during the cloud-collapse phase, $B \propto n^{2/3}$, is insufficient to provide the magnetic field strength to affect the first star formation.

A small-scale turbulent dynamo can lead further amplification (summarized in McKee et al. 2020). Cosmological magnetohydrodynamical (MHD) simulations provide power-law fits to their results that can be compared to the flux-freezing expression, specifically $B \propto n^{0.83}$ (Federrath et al. 2011) and $B \propto n^{0.89}$ (Turk et al. 2012). However, the amplification level via a turbulent small-scale dynamo depends on the numerical resolution (Sur et al. 2010, 2012). A recent MHD simulation (Stacy et al. 2022) showed that a small-scale dynamo could contribute only one or two orders of magnitude to the magnetic field amplification during gas cloud contraction. Hence, most of the amplification comes from compressional flux freezing.

Recently, Hirano et al. (2021) reported a new mechanism for magnetic field amplification during the protostellar accretion phase in primordial atomic-hydrogen (H) cooling gas clouds. Many fragments of a gravitationally unstable gas cloud amplify the magnetic field due to rotational motion and form a vital magnetic field region around the protostar. The simulations in Hirano et al. (2021) adopted the stiff equation of state (EOS) technique; we then could calculate the coupling between the high-density region and the magnetic field, which is essential in reproducing this amplification mechanism. However, MHD



Original content from this work may be used under the terms of the [Creative Commons Attribution 4.0 licence](#). Any further distribution of this work must maintain attribution to the author(s) and the title of the work, journal citation and DOI.

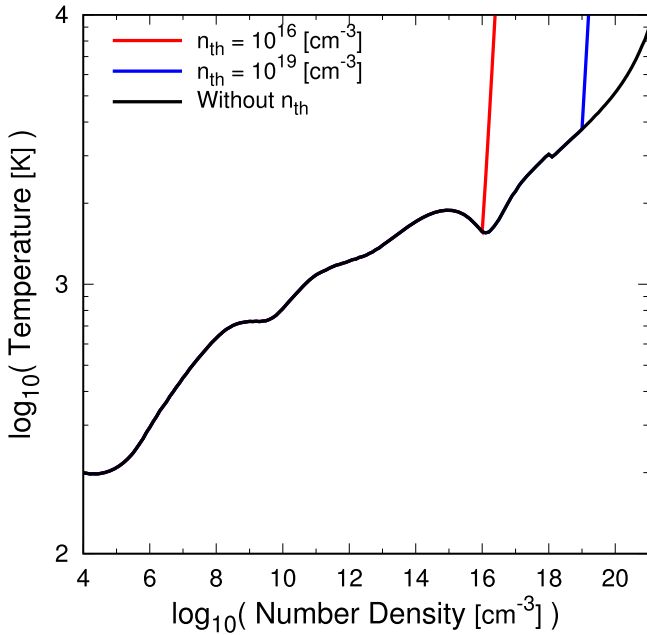


Figure 1. Thermal evolution models of the zero-metallicity star-forming clouds as a function of the gas number density. The black line is the base model theoretically obtained by the chemical reaction calculation (Omukai et al. 2008; Machida & Nakamura 2015). The colored lines, the adopted models in this study, are variants of the black line using the stiff-EOS technique with threshold density $n_{\text{th}} = 10^{16} \text{ cm}^{-3}$ (red) and 10^{19} cm^{-3} (blue), respectively.

simulations of the first star formation replaced the dense region by sink particles ($n_{\text{sink}} \sim 10^{13} \text{ cm}^{-3}$; Sharda et al. 2020, 2021; Stacy et al. 2022), which resulted in the loss of the magnetic field connection from the dense region. Therefore, it is not uncovered whether a similar amplification occurs in the primordial molecular-hydrogen (H_2) cooling gas clouds in such simulations. Our previous simulations (Machida & Doi 2013) assumed a relatively strong magnetic field (10^{-10} – 10^{-5} G at $n = 10^4 \text{ cm}^{-3}$) and did not consider a cosmologically weak magnetic field as an initial condition.

We performed three-dimensional ideal MHD simulations of the primordial star formation using the stiff-EOS technique. We find that exponential magnetic field amplification occurs in the vicinity of the protostar in the first three years after the first Population III protostars form and that the field-amplified region completely suppresses disk fragmentation. This Letter introduces this new exponential magnetic field amplification mechanism and substantial expansion of the amplified region. In Paper II, we will discuss the effects of model parameters on the first star formation in detail.

2. Methods

2.1. Numerical Methodology

We solve the ideal MHD equations with the barotropic EOS. Note that nonideal MHD effects are not effective in primordial gas clouds (e.g., Higuchi et al. 2018). To represent the thermal evolution in the zero-metallicity cloud, we adopt the EOS table based on a chemical reaction calculation (Omukai et al. 2008). Instead of the sink particle technique, we employ the stiff-EOS approach to represent the magnetic field structure connected to the dense gas region, which was established in our previous works (Machida & Doi 2013; Machida 2014; Hirano & Bromm 2017; Susa 2019; Hirano et al. 2021). Figure 1 shows

the resultant EOS tables. We adopt two threshold densities n_{th} to study the early amplification and later expansion of the magnetic field, respectively: (1) simulations until $t_{\text{ps}} = 100$ yr with $n_{\text{th}} = 10^{19} \text{ cm}^{-3}$, which reproduce hydrostatic cores whose radius is consistent with the mass–radius relation of an accreting primordial protostar (Hosokawa et al. 2010) and (2) until $t_{\text{ps}} = 1000$ yr with $n_{\text{th}} = 10^{16} \text{ cm}^{-3}$. We define the epoch of the first protostar formation ($t_{\text{ps}} = 0$ yr) to be when the gas number density first reached the threshold density ($n_{\text{max}} = n_{\text{th}}$).

We use the nested grid code (Machida & Nakamura 2015) in which the rectangular grids of $(n_x, n_y, n_z) = (256, 256, 32)$ are superimposed. The base grid has box size $L(0) = 9.83 \times 10^5$ au and cell size $h(0) = 3.84 \times 10^3$ au. A new finer grid is generated to resolve the Jeans wavelength by at least 32 cells. The maximum grid levels and the finest cell sizes are $l = 17$ and $h(17) = 0.0293$ au for runs with $n_{\text{th}} = 10^{19} \text{ cm}^{-3}$, whereas $l = 14$ and $h(14) = 0.234$ au for $n_{\text{th}} = 10^{16} \text{ cm}^{-3}$, respectively.

2.2. Initial Condition

The initial cloud has an enhanced Bonner–Ebert (BE) density profile $n(r) = f \cdot n_{\text{BE}}(r)$ with an enhanced factor $f = 1.6$ to promote cloud contraction. The initial central density is $f \cdot n_{\text{BE}}(r=0) = f \cdot 10^4 \text{ cm}^{-3}$. The mass and size of the initial cloud are $M_{\text{cl},0} = 4.83 \times 10^3 M_{\odot}$ and $R_{\text{cl},0} = 2.38$ pc, respectively. A rigid rotation of $\Omega_0 = 1.31 \times 10^{-14} \text{ s}^{-1}$ is imposed. With these settings, the ratio of the thermal and rotational energies to the gravitational energy of the initial cloud are $\alpha_0 = 0.533$ and $\beta_0 = 0.0209$, respectively. We do not include turbulence and do not consider a small-scale dynamo (e.g., Sur et al. 2010; McKee et al. 2020) because we only consider very weak fields, which are significantly amplified by the rotation motion of protostars (see Section 4 for details).

2.3. Model Parameter

We impose a uniform magnetic field B_0 with the same direction as the initial cloud’s rotation axis in the whole computational domain. We examine the parameter dependence of the first star formation on $B_0 = 0, 10^{-20}, 10^{-15},$ and 10^{-10} G (labeled B00, B20, B15, and B10). We adopt B20 as the fiducial model in this study because $B_0 = 10^{-20}$ G is lower than the cosmological value $\sim 10^{-18}$ G (Ichiki et al. 2006). If we can show that magnetic fields affect first star formation in this model, we can prove that the first stars cannot avoid the effects of magnetic fields. By comparing B20 with B00, we examine the magnetic effect on the first star formation. By comparing B20 with B15 and B10, we study the necessity of the early amplification of the magnetic field strength before the star-forming cloud formation.

3. Results

This section shows the results of MHD simulations with different initial magnetic field strengths (B00, B20, B15, and B10). We run four models under different threshold densities until $t_{\text{ps}} = 100$ yr ($n_{\text{th}} = 10^{19} \text{ cm}^{-3}$) and 1000 yr ($n_{\text{th}} = 10^{16} \text{ cm}^{-3}$). Because the calculation results among models with different resolutions converged outside the resolution limit,³ this section shows the combined results of the first 100 yr under $n_{\text{th}} = 10^{19} \text{ cm}^{-3}$ and the latter 900 yr under $n_{\text{th}} = 10^{16} \text{ cm}^{-3}$.

³ We find no resolution-dependent effects like magneto-rotational instability (MRI) in our simulations.

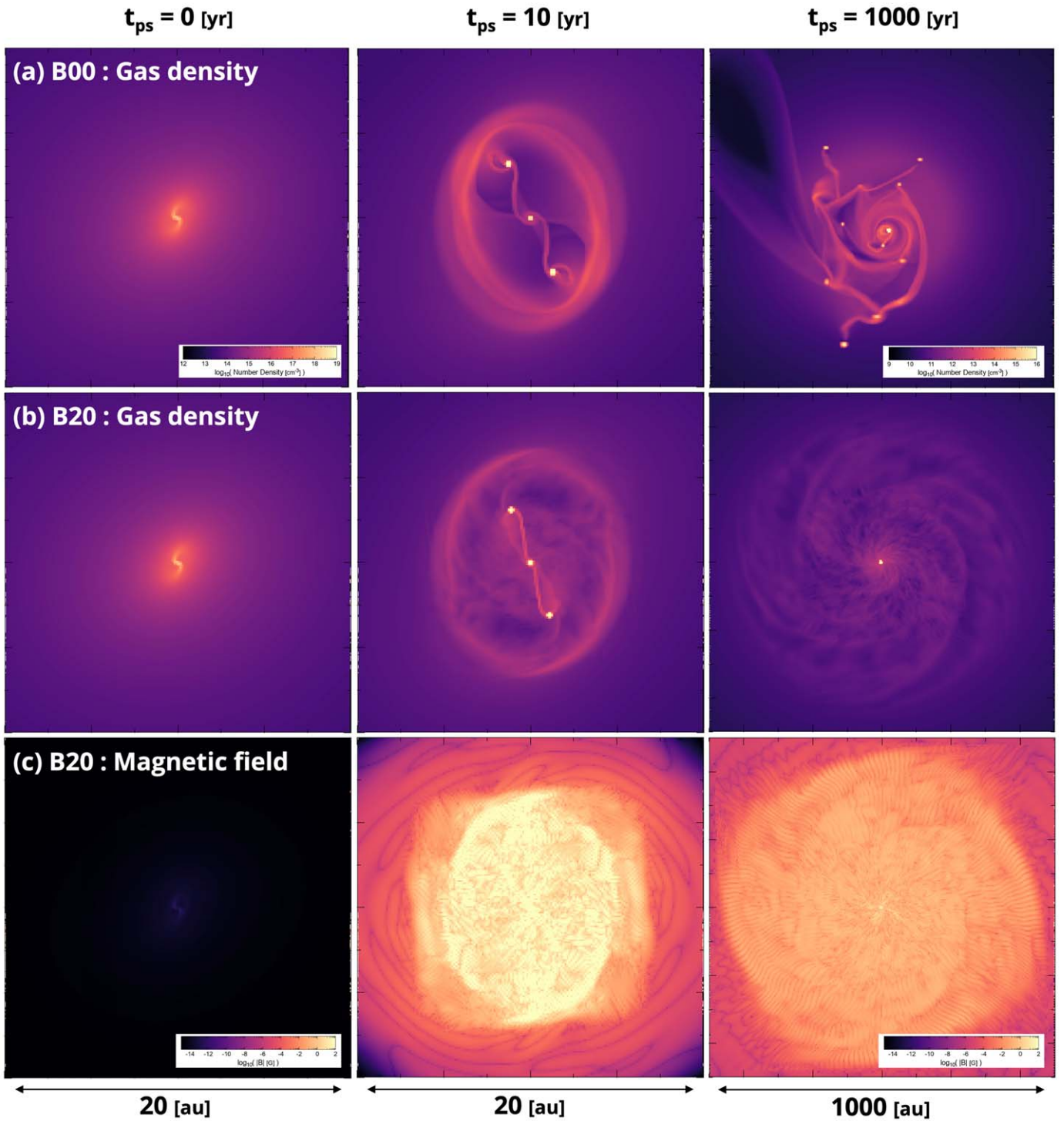


Figure 2. Cross-sectional view on the $z = 0$ plane around the most massive protostar at $t_{ps} = 0, 10,$ and 1000 yr after the first protostar formation from left to right. Panels: (top) gas number density in model B00, (middle) gas number density in model B20, and (bottom) absolute magnetic field strength in model B20. The box sizes are 20 au in the left and middle panels and 1000 au in right panels, respectively.

3.1. Fiducial Model

Figure 2 compares the simulation results of the fiducial model (B20) and the unmagnetized model (B00) during the first 1000 yr of the protostar accretion phase. At the birth time of the first protostar (left panels), the density structure around the protostar is identical because the magnetic field strength in the vicinity of the protostar is too weak (pico-Gauss = 10^{-12} G at most) to affect the collapsing gas cloud. However, after a

decade (middle column in Figure 2), the magnetic field strength on the primary protostar surface ($\sim 30 R_{\odot}$) amplifies to kilo-Gauss (similar to the Population I protostars; Johns-Krull 2007), and this strong “seed” field amplifies the surrounding field in a region of 10 au radius. Within this strong magnetic field region, the density and velocity structure of the accretion gas are affected by the magnetic field. After 1000 yr (right column in Figure 2), the amplified magnetic field region extends to a

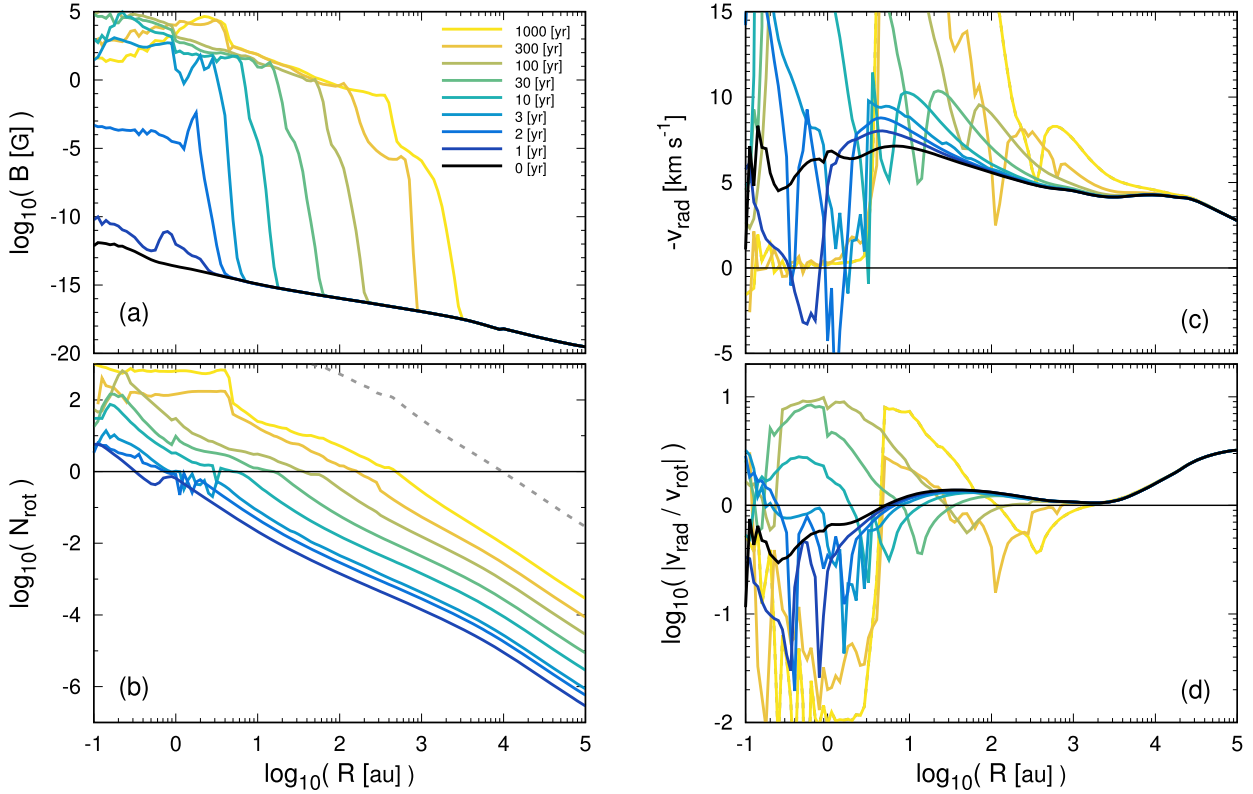


Figure 3. Radial profiles for model B20 at $t_{ps} = 0, 1, 2, 3, 10, 30, 100, 300,$ and 1000 yr after the formation of the first protostar. Panels: (a) magnetic field strength, (b) number of orbital rotations at t_{ps} , $N_{\text{rot}} = (v_{\text{rot}} t_{ps}) / (2\pi R)$, (c) radial velocity, and (d) absolute value of the ratio of the radial velocity to the rotational velocity. The line for $t_{ps} = 0$ yr is not plotted in panel (b) because $N_{\text{rot}} = 0$ for every R at $t_{ps} = 0$ yr. The dotted line in panel (b) represents the expected N_{rot} at $t_{ps} = 10^5$ yr when the first star ends its accretion phase (Figure 1 in Hirano & Bromm 2017) by using the radial profile of rotational velocity at $t_{ps} = 1000$ yr. The horizontal lines indicate $N_{\text{rot}} = 1$ in panel (b), $-v_{\text{rad}} = 0$ in panel (c), and $|v_{\text{rad}}| = |v_{\text{rot}}|$ in panel (d).

radius of about 500 au and multiple protostars that appeared in the unmagnetized model have disappeared in the fiducial model. The global spiral structure of gas appears inside the amplified region due to the angular momentum transport by magnetic braking that allows accretion to proceed efficiently.

The origin of this exponential magnetic field amplification from 10^{-12} G to 10^3 G in nearby protostars is rapid rotational motion capable of winding up magnetic fields. The magnetic field strength in the vicinity of the protostar has been sufficiently amplified in the first 3 yr after protostar formation (Figure 3(a)). In the region of ≤ 10 au, the number of orbital rotations exceeds one at $t_{ps} = 0$ yr and reaches several dozen at $t_{ps} = 3$ yr (Figure 3(b)). The magnetic field amplification region then widens over time, and its arrival radius equals the radius at which the orbital rotation rate exceeds one, $N_{\text{rot}} = 1$. Figure 3(c) shows the negative radial velocity $-v_{\text{rad}}$ and indicates that the amplified field cannot significantly impede the gas accretion into the central region. Figure 3(d) plots the ratio of the radial velocity to the rotational (or azimuthal) velocity. The figure shows that the gas falls toward the center while rotating. These figures mean that gravitational energy is efficiently converted into magnetic energy through kinetic (or rotational) energy after the formation of the first protostar. We expect that the amplified magnetic field region could spread about 10^4 au ~ 0.05 pc, inside which the total gas mass is about $\sim 500 M_{\odot}$ in this model, until the end of the accretion phase of the first stars (about 10^5 yr; dotted line).

How does this exponentially amplifying magnetic field affect the formation process of the first stars? The amplified magnetic field eliminates fragmentation of the gravitationally unstable

accretion disk, and a single protostar forms at the center of the cloud (Figure 4(a)). On the other hand, the stellar masses are not different between magnetized and unmagnetized models (Figure 4(b)). In any case, the fragments born in the vicinity of the protostar will merge immediately. The rotation velocities, the second important parameter of the stellar evolution theory, are nearly constant, ~ 0.05 times the Keplerian velocity, regardless of the models and evolution time (Figure 4(c)). Because the rotational degree is low, it seems reasonable to adopt a nonrotational model for the stellar evolution (e.g., Yoon et al. 2012).

3.2. Dependence on the Initial B-field Strength

We simulated two comparison models (B15 and B10) with higher initial magnetic field strengths than the fiducial model to examine the effects of other amplification mechanisms, which do not appear in our simulations. The evolution of a collapsing gas cloud is almost similar among the three models until $t_{ps} = 0$ yr except for the magnetic field strength distribution. Figure 5 shows that, in both cases, exponential magnetic field amplification occurs immediately after $t_{ps} = 0$ yr, similar to the fiducial model. Because the expansion of the amplified magnetic field region completely prevents disk fragmentation, all magnetized models show the same results: the formation of a single first star (Figure 4(a)).

4. Discussion

The magnetic field amplification after protostar formation proceeds in the following steps: (1) The rotational motion of

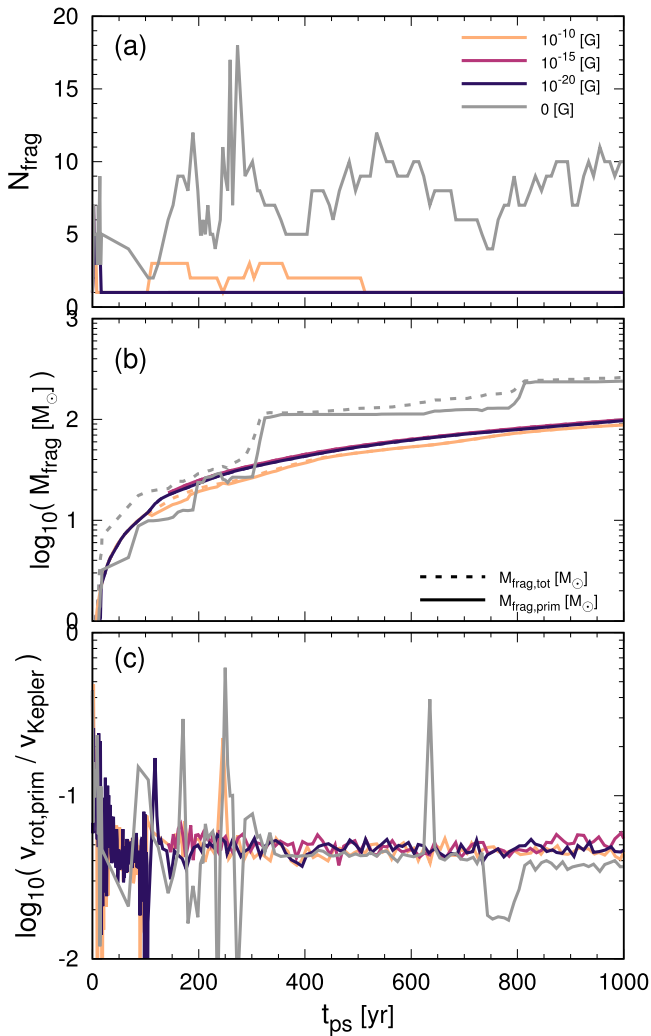


Figure 4. Time evolution of the protostar properties for models B00 (gray), B20 (blue), B15 (red), and B10 (yellow). Panels: (a) number of protostars, (b) total mass of protostars $M_{frag,tot}$ and mass of the most massive (primary) protostar $M_{frag,prim}$, and (c) ratio of rotational velocity to the Keplerian velocity of the primary protostar.

protostars amplifies the small magnetic field around them. (2) The amplification rate of the magnetic field in the surrounding region increases according to the induction equation, $\partial B / \partial t = \nabla \times (\mathbf{v} \times \mathbf{B})$. (3) The rotation-dominated region gradually extends outward, where the magnetic field is amplified by mechanism (1). The MHD simulations adopting the sink particle technique cannot reproduce the “seed” magnetic field amplification around the protostar and the following propagation outwards because the rotation of the high-density region does not couple with the magnetic field.

The high accretion rate in the atomic-hydrogen (H) cooling halo causes many fragments, which amplify the magnetic field due to the rotation (Hirano et al. 2021). In the molecular-hydrogen (H_2) cooling halo investigated in this study, the disk fragments appear only at the initial stage but soon merge into the primary protostar. The orbital rotation around the protostar alone can amplify the magnetic field without further fragmentation. This amplification mechanism is unique to star formation in the early universe because it does not occur in nearby star-forming regions where the magnetic field saturates

before the protostar accretion phase. Thus, the feedback cannot be ignored under a strong magnetic field environment.

This magnetic field amplification prohibits the fragmentation of the accretion disk. If the star-forming gas cloud has a sufficient rotational degree, a gravitationally unstable accretion disk forms and fragments, but the amplified magnetic field immediately suppresses disk fragmentation. Conversely, if the rotation of the gas cloud is weak, the amplification of the magnetic field by the rotation is less efficient. In this case, a gravitationally unstable accretion disk cannot form, and disk fragmentation does not occur. In either case, a single first star remains.

We provide some caution regarding the rotational amplification of the magnetic field. Recent studies have suggested turbulence as an amplification mechanism of the magnetic field and shown that disk fragmentation is not significantly suppressed in turbulent environments (e.g., Sharda et al. 2021; Prole et al. 2022). We did not consider turbulence in this study (Section 2.2). The rotational amplification mechanism may not be effective in highly turbulent environments because the turbulent reconnection (or reconnection diffusion) breaks the coupling between the magnetic field and gas (or fluid motion) even in ideal MHD calculations (e.g., Lazarian & Vishniac 1999; Lazarian et al. 2020). Thus, the existence of (strong) turbulence may significantly change our results, which will be investigated in our future paper. In addition, rotational amplification would not be efficient when magnetic dissipation, such as ambipolar diffusion and ohmic dissipation, is effective, and the amplified field significantly dissipates. As shown in Higuchi et al. (2018), ambipolar diffusion becomes effective in the high-density region ($n \gtrsim 10^{12} \text{ cm}^{-3}$) when the magnetic field strength exceeds $B \gtrsim 0.1\text{--}1$ kG. Thus, we need to consider ambipolar diffusion in a further evolutionary stage.

Next, we discuss the amplification of the magnetic field and the treatment of protostars. We have used the stiff-EOS technique instead of the sink particle technique, as in our previous studies (e.g., Machida & Doi 2013; Machida & Nakamura 2015; Hirano et al. 2021), because some physical quantities related to the amplification or accumulation of the magnetic field (or flux), such as the mass-to-flux ratio and kinetic energy, can be conserved. The sink particle technique removes only the gas around the sink particles without removing magnetic flux. Thus, the mass-to-flux ratio is not conserved and would decrease with time. With a small mass-to-flux ratio, the magnetic flux is leaked out from the region around the sink particle, for example, due to interchange instability (Zhao et al. 2011; Machida & Basu 2020). We also showed that rotation around protostars amplifies the magnetic field. However, the rotational energy, which is proportional to the mass, is substantially removed with the sink particle technique. In addition, the high-density gas is not coupled to the magnetic field after removing the gas. Thus, the rotational amplification of the magnetic field should be underestimated with the sink particle technique. For these reasons, we used the stiff-EOS technique. It is expected that the difference in the results among recent studies (rare or frequent fragmentation) can be attributed to the treatment of protostars (sink particle or stiff-EOS techniques) and the inclusion of turbulence.

Finally, we comment on observational constraints of the first stars. Our result is consistent with the observational constraint with no observation of low-mass ($< 0.8 M_{\odot}$) surviving first stars in the galaxy. Though the amplified magnetic field prohibits small-mass disk fragmentation, it is unclear whether the

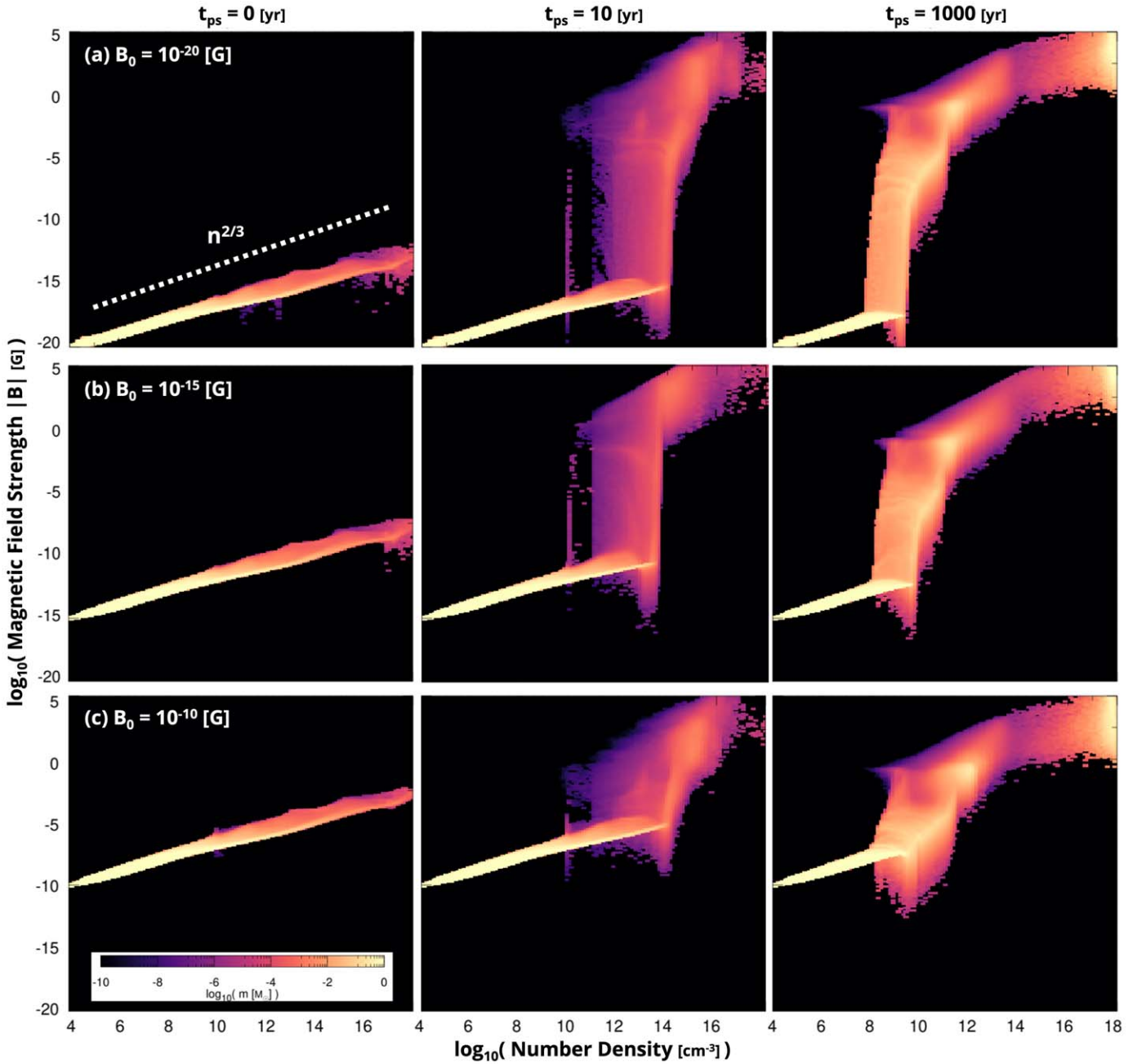


Figure 5. Phase diagrams of the absolute magnetic field strength for models B20, B15, and B10 (top to bottom) at $t_{\text{ps}} = 0, 10,$ and 1000 yr after the first protostar formation (left to right). The white dotted line in the top-left panel shows the power law $B \propto n^{2/3}$ through flux freezing during the cloud compression.

magnetic field affects wide binaries/multiples (separation $> 10^3$ au; Sugimura et al. 2020) and chemothermal instability at the Jeans scale (Hirano et al. 2018), which form more massive fragments. If a massive first star binary forms from them, it could leave the massive star binary, which can be a promising progenitor of BH–BH mergers like the gravitational-wave sources (Kinugawa et al. 2014). We are interested in the contribution of the amplified magnetic field to the contraction of the binary orbit, but it is outside the scope of this study.

5. Conclusion

We introduce a new exponential amplification mechanism of the magnetic field during the accretion phase of the first star formation. Even if the star-forming gas cloud only has

cosmological magnetic field strength, the orbital rotation around the protostar amplifies the tiny magnetic seed to kilo-Gauss as the current protostar in less than 10 yr after the protostar formation. The amplified magnetic field region expands during the accretion phase and reaches $\sim 10^4$ au (inside which $\sim 500 M_{\odot}$) at $t_{\text{ps}} \sim 10^5$ yr when the protostar becomes a zero-age main-sequence star. Because the strong magnetic field completely prevents disk fragmentation, only one protostar forms in each accretion disk. We conclude that the first star formation is inevitably affected by magnetic fields even if the initial magnetic field strength has a cosmological value, about 10^{-18} G.



Hirano et al. (2021) showed the magnetic field amplification in the atomic-hydrogen (H) cooling gas clouds. This Letter

shows that the same amplification also occurs in molecular-hydrogen (H_2) cooling gas clouds with lower accretion rates and a limited number of fragments. Paper II will discuss in detail how the effects on gas cloud evolution depend on the initial magnetic field strength. We note that the magnetic field amplification shown in this study would not operate in contemporary star formation because the magnetic field significantly dissipates within the disk. For this reason, we have overlooked this mechanism until today.

In the future, we will perform a parameter survey of the MHD simulations for the parameter ranges of the primordial star-forming gas clouds obtained from the cosmological simulations (Hirano et al. 2014, 2015). Although disk fragmentation is wholly eliminated in this study, we will check whether or not gas clouds with different physical parameters, such as accretion rate and rotation degree, result in the same. In addition, the current simulations end at $t_{\text{ps}} = 1000$ yr, and additional calculations are needed to determine the final stellar mass at $t_{\text{ps}} \sim 10^5$ yr when the first star reaches the zero main-sequence stage. In the future, we will fully update the theory of first star formation to incorporate MHD effects and determine the formation rates of observational counterparts, such as low-mass surviving stars and massive BH binaries.

This work used the computational resources of the HPCI system provided by the supercomputer system SX-Aurora TSUBASA at Cyberscience Center, Tohoku University, and Cybermedia Center, Osaka University through the HPCI System Research Project (Project ID: hp210004 and hp220003), and Earth Simulator at JAMSTEC provided by 2021 and 2022 Koubo Kadai. S.H. was supported by JSPS KAKENHI grant Nos. JP18H05222, JJP21K13960, and JP21H01123 and Qdai-jump Research Program 02217. M.N.M. was supported by JSPS KAKENHI grant Nos. JP17K05387, JP17KK0096, JP21K03617, and JP21H00046 and University Research Support Grant 2019 from the National Astronomical Observatory of Japan (NAOJ).

ORCID iDs

Shingo Hirano  <https://orcid.org/0000-0002-4317-767X>
Masahiro N. Machida  <https://orcid.org/0000-0002-0963-0872>

References

- Federrath, C., Sur, S., Schleicher, D. R. G., Banerjee, R., & Klessen, R. S. 2011, *ApJ*, **731**, 62
- Greif, T. H. 2015, *ComAC*, **2**, 3
- Higuchi, K., Machida, M. N., & Susa, H. 2018, *MNRAS*, **475**, 3331
- Hirano, S., & Bromm, V. 2017, *MNRAS*, **470**, 898
- Hirano, S., & Bromm, V. 2018, *MNRAS*, **476**, 3964
- Hirano, S., Hosokawa, T., Yoshida, N., et al. 2014, *ApJ*, **781**, 60
- Hirano, S., Hosokawa, T., Yoshida, N., Omukai, K., & Yorke, H. W. 2015, *MNRAS*, **448**, 568
- Hirano, S., Machida, M. N., & Basu, S. 2021, *ApJ*, **917**, 34
- Hirano, S., Yoshida, N., Sakurai, Y., & Fujii, M. S. 2018, *ApJ*, **855**, 17
- Hosokawa, T., Yorke, H. W., & Omukai, K. 2010, *ApJ*, **721**, 478
- Ichiki, K., Takahashi, K., Ohno, H., Hanayama, H., & Sugiyama, N. 2006, *Sci*, **311**, 827
- Inayoshi, K., Visbal, E., & Haiman, Z. 2020, *ARA&A*, **58**, 27
- Johns-Krull, C. M. 2007, *ApJ*, **664**, 975
- Kinugawa, T., Inayoshi, K., Hotokezaka, K., Nakauchi, D., & Nakamura, T. 2014, *MNRAS*, **442**, 2963
- Koh, D., Abel, T., & Jedamzik, K. 2021, *ApJL*, **909**, L21
- Lazarian, A., Eyink, G. L., Jafari, A., et al. 2020, *PhPI*, **27**, 012305
- Lazarian, A., & Vishniac, E. T. 1999, *ApJ*, **517**, 700
- Machida, M. N. 2014, *ApJL*, **796**, L17
- Machida, M. N., & Basu, S. 2020, *MNRAS*, **494**, 827
- Machida, M. N., & Doi, K. 2013, *MNRAS*, **435**, 3283
- Machida, M. N., & Nakamura, T. 2015, *MNRAS*, **448**, 1405
- Magg, M., Hartwig, T., Agarwal, B., et al. 2018, *MNRAS*, **473**, 5308
- McKee, C. F., Stacy, A., & Li, P. S. 2020, *MNRAS*, **496**, 5528
- Omukai, K., Schneider, R., & Haiman, Z. 2008, *ApJ*, **686**, 801
- Prole, L., Clark, P., Klessen, R., Glover, S., & Pakmor, R. 2022, arXiv:2206.11919
- Sadanari, K. E., Omukai, K., Sugimura, K., Matsumoto, T., & Tomida, K. 2021, *MNRAS*, **505**, 4197
- Sharda, P., Federrath, C., & Krumholz, M. R. 2020, *MNRAS*, **497**, 336
- Sharda, P., Federrath, C., Krumholz, M. R., & Schleicher, D. R. G. 2021, *MNRAS*, **503**, 2014
- Stacy, A., McKee, C. F., Lee, A. T., Klein, R. I., & Li, P. S. 2022, *MNRAS*, **511**, 5042
- Sugimura, K., Matsumoto, T., Hosokawa, T., Hirano, S., & Omukai, K. 2020, *ApJL*, **892**, L14
- Sur, S., Federrath, C., Schleicher, D. R. G., Banerjee, R., & Klessen, R. S. 2012, *MNRAS*, **423**, 3148
- Sur, S., Schleicher, D. R. G., Banerjee, R., Federrath, C., & Klessen, R. S. 2010, *ApJL*, **721**, L134
- Susa, H. 2019, *ApJ*, **877**, 99
- Turk, M. J., Oishi, J. S., Abel, T., & Bryan, G. L. 2012, *ApJ*, **745**, 154
- Yoon, S. C., Dierks, A., & Langer, N. 2012, *A&A*, **542**, A113
- Zhao, B., Li, Z.-Y., Nakamura, F., Krasnopolsky, R., & Shang, H. 2011, *ApJ*, **742**, 10